Journal of Cancer Research and Clinical Oncology (2019) 145:2951–2967
https://doi.org/10.1007/s00432-019-03051-6

ORIGINAL ARTICLE – CANCER RESEARCH

Therapeutic delivery of microRNA-143 by cationic lipoplexes for non-small cell lung cancer treatment in vivo

Qianqian Jiang[1] · Yue Yuan[1] · Yi Gong[1] · Xinmei Luo[1] · Xiaolan Su[1] · Xueting Hu[1] · Wen Zhu[1]

Received: 20 June 2019 / Accepted: 4 October 2019 / Published online: 25 October 2019

Abstract

Purpose Non-small cell lung cancer (NSCLC) remains the leading cause of cancer-related deaths worldwide and new improvements are urgently needed. Several miRNA-targeted therapeutics have reached clinical development. MicroRNA-143 (miR-143) was found to significantly suppress the migration and invasion of NSCLC. It might be of great potential for NSCLC treatment. However, the therapeutic effect of miR-143 against NSCLC in vivo has not been explored until now.

Methods The cationic liposome/pVAX-miR-143 complex (CL-pVAX-miR-143) was prepared and its biodistribution was assessed. The tumor suppression effects of CL-pVAX-miR-143 were evaluated in early-stage and advanced experimental lung cancer metastasis mice models by systemic delivery, respectively, and also in subcutaneous tumor models by intratumoral injection. The toxicity of CL-pVAX-miR-143 was assessed by H&E analysis and biochemical measurements. The preliminary mechanism of CL-pVAX-miR-143 on tumor suppression was explored by immunochemistry and western blotting.

Results The assays on the stability and safety of CL-pVAX-miR-143 showed that it mainly accumulated in the lung after systemic administration. The intratumoral delivery of CL-pVAX-miR-143 effectively inhibited A549 subcutaneous tumor growth. Notably, systemic delivery of CL-pVAX-miR-143 significantly inhibited tumor metastasis and prolonged survival dose dependently in early-stage experimental lung cancer metastasis models. More importantly, same results were shown in advanced mice models with metastasis. CL-pVAX-miR-143 treatment did not induce obvious acute toxicity. The preliminary mechanism on inhibiting tumor metastasis might be induced by targeting CD44v3.

Conclusions Our results suggested that CL-pVAX-miR-143 might be a promising strategy for clinical treatment of non-small cell lung cancer, especially for advanced NSCLC with metastasis.

Keywords NSCLC · miR-143 · Advanced cancer · Early-stage cancer · Tumor metastasis and growth · Cationic liposome

Introduction

Lung cancer is the leading cause of cancer death among males and females (Siegel et al. 2019). The vast majority of lung cancer patients are diagnosed at an advanced stage (Zugazagoitia et al. 2017). And over 80% of the patients diagnosed with lung cancer present with metastatic disease (Hirsch et al. 2016). Although surgery, radiation therapy, chemotherapy and new target treatments can control most of the primary tumors effectively (Hirsch et al. 2017), these treatments have limited utility in curbing the metastatic spread of cancer cells and in metastatic patients (Steeg 2006; Zer and Leighl 2014). Statistics show that the 5-year survival rate is only 5% with those distant metastatic lung cancer patients (Siegel et al. 2019). Thus, it is of great significance to further develop effective therapeutic methods to improve the survival rates of lung cancer patients.

MicroRNAs (miRNAs) are noncoding, 21–23 nucleotides RNAs that negatively regulate gene expression by binding to the 3′ untranslated regions (3′UTRs) of target transcripts, leading to mRNA degradation, or inhibiting mRNA translation (Hosseinahli et al. 2018). MiRNAs are the master switches in gene regulation and have been confirmed to be involved in many biological processes, such as cell proliferation, differentiation and apoptosis, and play crucial roles in

Qianqian Jiang and Yue Yuan contributed equally to this work.

✉ Wen Zhu
zhuwen@scu.edu.cn

[1] State Key Laboratory of Biotherapy and Cancer Center, West China Hospital, Sichuan University/Collaborative Innovation Center of Biotherapy, No. 1, Keyuan 4th Road, Gaopeng Street, High Technological Development Zone, Chengdu 610041, Sichuan, China

the regulation of tumor development and progression (Lu et al. 2018). Importantly, a single miRNA may target multiple mRNAs. As a result, miRNA-mediated regulation can coordinately affect hundreds of targets, which form a dedicated regulatory net; thus, miRNAs might act as promising potential targets for the therapy of lung cancer patients (Lu et al. 2018). Currently, "miRNA replacement therapy" has made great progresses (Hosseinahli et al. 2018; Rupaimoole and Slack 2017). For example, TargomiR trials with miR-16 had been completed successfully without inducing toxicity or adverse immune responses, and were expected to enter phase II trial (van Zandwijk et al. 2017).

Recent advances demonstrated that miRNAs were also related with cancer metastasis, and further experiments on miRNA replacement therapy have also been validated. Researches showed that metastatic cancers like colorectal cancer (Wang et al. 2016), hepatocellular carcinoma (Zheng et al. 2015), prostate cancer (Iscaife et al. 2018) were inhibited by restoring the miRNA expression. Among those miRNAs, miR-143 was reported downregulated in many cancers (He et al. 2016; Jin et al. 2018; Lei et al. 2017), which could target many important genes involved in tumor growth or metastasis (Karmakar et al. 2017; Noguchi et al. 2011; Zhai et al. 2017).

In recent years, although there was an interesting debate on the role of miR-143/145 in lung cancer development (Dimitrova et al. 2016; Cioce et al. 2016), a series of studies have demonstrated that miR-143 was downregulated in lung cancer tissues and cell lines and related with cancer development (Skjefstad et al. 2018; Võsa et al. 2013; Wang et al. 2017). Our previous research found the notable downregulation of miR-143 in NSCLC tissues and cell lines, and that miR-143 could significantly affect migration and invasion of lung cancer both in vitro and in vivo, which might through targeting CD44v3 (Ma et al. 2013). Moreover, miR-143 specifically targeted CDK1 in lung cancer cells, and combinatorial transfection of miR-143 and miR-506 could inhibit lung cancer cell cycle progression and angiogenesis (Hossian et al. 2018). In addition, overexpression of miR-143 downregulated gefitinib-resistant NSCLC cell proliferation, promoted apoptosis, and suppressed the phosphorylation of EGFR, AKT, and ERK1/2 (Dong and Hu 2018). These findings indicated that miR-143 might be of great potential for treating lung cancer. However, the therapeutic effect of miR-143 against lung cancer has not been explored until now. Therefore, in this study, we hypothesized that miRNA-143 could be used as an effective therapeutic "drug" in NSCLC in vivo. We firstly prepared cationic liposome/pVAX-miR-143 complexes (CL-pVAX-miR-143) and its biodistribution was assessed. Subsequently, the tumor suppression effects of CL-pVAX-miR-143 were evaluated in early-stage and advanced experimental lung cancer metastasis mice models by systemic delivery, respectively, and also in subcutaneous tumor models by intratumoral injection. Furthermore, the toxicity of CL-pVAX-miR-143 and the preliminary mechanism of CL-pVAX-miR-143 on tumor suppression was also explored.

Results

Characterization of CL-pVAX-miR-143

To evaluate the encapsulation efficiency of cationic liposome (CL), the gel retardation assay was conducted. The result showed that cationic liposomes were able to bind to pVAX-miR-143 plasmids through electrostatic interaction. Complete retardation of pVAX-miR-143 was achieved when the weight ratio of cationic liposome versus pVAX-miR-143 was over 2 (Fig. 1a).

It is reported that particle size, the surface charge of cationic liposome could affect cell uptake and targeting (Schroeder et al. 2012). Thus, we measured the sizes and zeta potentials of CL-pVAX-miR-143. The results showed that as the weight ratio was elevated, the size was decreased from 261.85 ± 8.85 nm to 129.5 ± 0.1 nm, while the zeta potential was increased from 25.9 ± 2.2 mV to 31.9 ± 1.9 mV (Fig. 1b). When the weight ratio was 4, the CL-pVAX-miR-143 was 204.65 ± 3.55 nm in size, with a zeta potential of 31.45 ± 0.35 mV. Besides, different ratios of cationic liposome/EGFP complexes were prepared to test the transfection efficiency, and the results showed that the complexes with the weight ratio of 4 possessed higher transfection efficiency (Fig. 1c).

Cationic liposome often causes red blood cell aggregation due to its high positive charge. However, we found that CL-pVAX-miR-143 complex with the zeta potential from -20 to 31 mV did not aggregate red blood cells in 0.5% blood cell suspension, and this might be related with the suitable zeta potential (Fig. 1d). Subsequently, the stability of CL-pVAX-miR-143 in DNase I and serum was also tested. The results showed that CL-pVAX-miR-143 was stable and pVAX-miR-143 plasmid was protected from degradation in serum and DNase I in 2 h, compared to the pVAX-miR-143 (Fig. 1e, f). As we know, particles tend to reside in the lungs during the first 1–2 h post-administration (Schroeder et al. 2012), which may support that our complexes were suitable for in vivo application in the lung. Thus, the CL-pVAX-miR-143 with the weight ratio of 4 was selected to apply in the following experiments.

Biodistribution of systemically delivered CL-pVAX-miR-143

To evaluate the biodistribution of CL-pVAX-miR-143, mice were killed 24 h after the systemic administration of

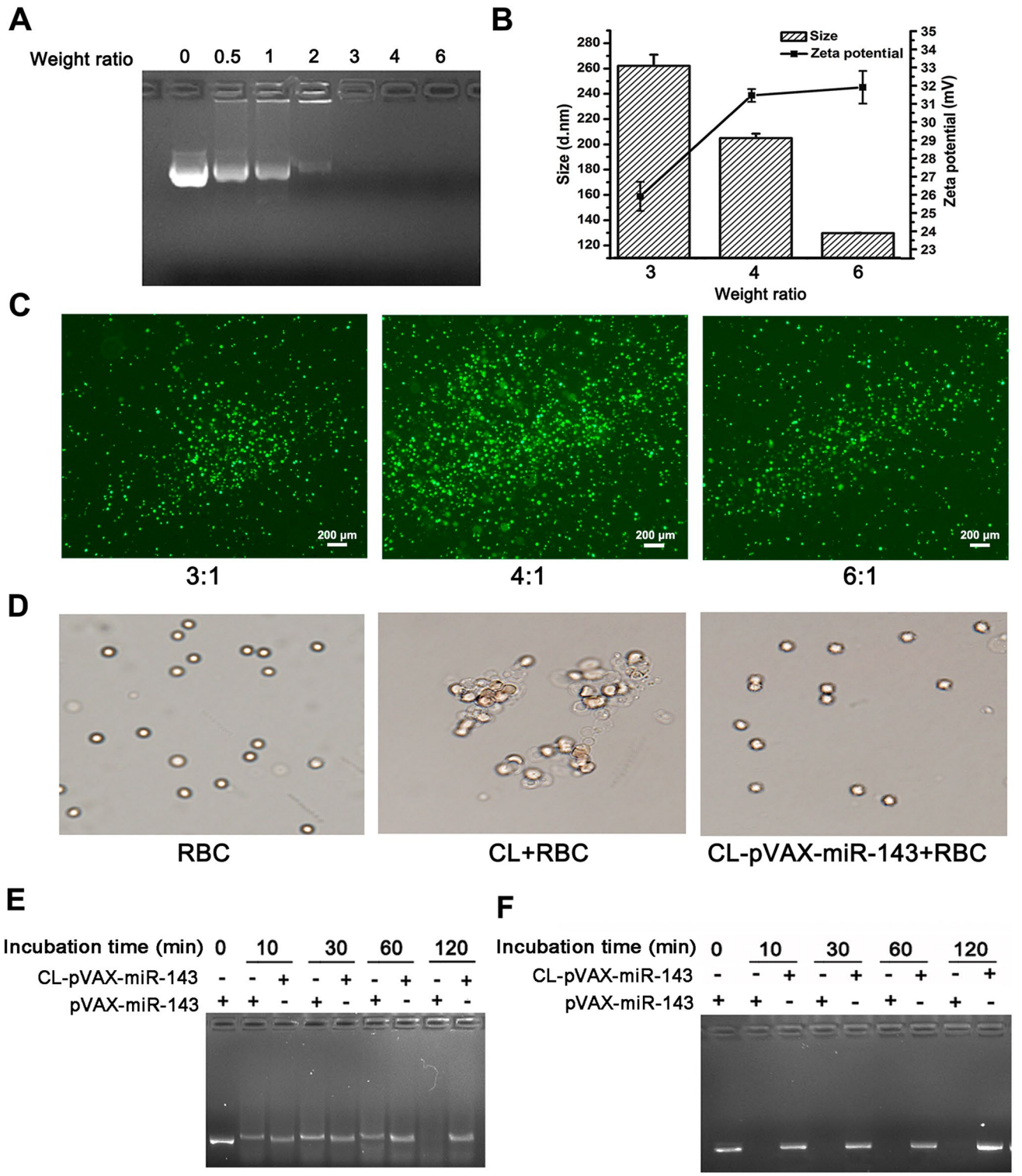

Fig. 1 Characterization of cationic liposome/miR-143 complexes (CL-pVAX-miR-143). **a** Agarose gel electrophoresis retardation assay of miR-143 with cationic liposome at different weight ratio; **b** size and zeta potential of CL-pVAX-miR-143 at different weight ratio; **c** transfection efficiency of cationic liposome/EGFP. Scale bar: 200 μm; **d** the morphology of red blood cells after incubating with CL-pVAX-miR-143; **e** agarose gel electrophoresis of CL-pVAX-miR-143 in the presence of serum; **f** agarose gel electrophoresis of CL-pVAX-miR-143 in the presence of DNase I

CL-pVAX-miR-143, major organs were collected and RNA was isolated from all tissues. Then, qRT-PCR was used to detect the expression levels of miR-143 in major organs (heart, liver, spleen, lung, and kidney) (Daige et al. 2014). The result showed that the expression level of miR-143 was most notably elevated in the lung compared with that in other organs, which indicated that CL-pVAX-miR-143 was mainly accumulated and expressed in the lung after systemic delivery (Fig. 2). Consequently, our results revealed that systemic delivery of CL-pVAX-miR-143 was suitable for lung cancer therapy in vivo.

Systemic delivery of CL-pVAX-miR-143 inhibited tumor metastasis in lung cancer xenografts at early stage

To evaluate the tumor suppression effects of CL-pVAX-miR-143 in early-stage experimental A549 lung cancer metastasis mice model, the mice were treated with 5% Glc, CL-pVAX, different doses of CL-pVAX-miR-143 or cisplatin, respectively, when minor lung metastatic tumor nodules were observed on the lung after cells engraftment for 2 weeks (Fig. 3a). Results showed that compared with 5% Glucose (Glc) treatment, the reductions of tumor metastasis nodules with treatment of cisplatin or CL-pVAX-miR-143 (0.5 mg/kg, 1 mg/kg) were 50.6%, 68.2% and 87.6%, respectively, which demonstrated that treatment with cisplatin or different doses of CL-pVAX-miR-143 all showed obvious inhibition of tumor metastasis ($P < 0.01$). Moreover, the CL-pVAX-miR-143 (1 mg/kg) treatment showed an enhanced reduction compared with 5% Glc or CL-pVAX treatment ($P < 0.001$), and also showed significantly statistical difference compared with cisplatin treatment ($P < 0.05$) (Fig. 3b, c). Likewise, HE staining of lung tissue sections also demonstrated that CL-pVAX-miR-143-treated lungs had much fewer and smaller tumor nodules compared with the controls (Fig. 3d), and the therapeutic effects showed to be dose dependent.

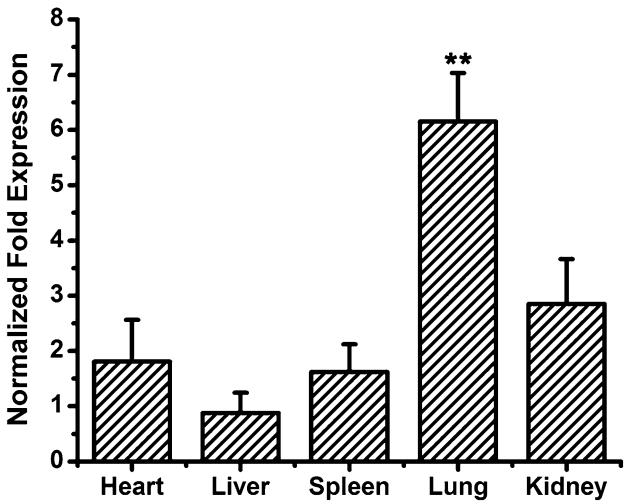

Fig. 2 Biodistribution of CL-pVAX-miR-143 in major organs after systemic administration of Balb/c mice was systemically injected with 5% Glc ($n = 4$) or one single dose of 1 mg/kg CL-pVAX-miR-143 ($n = 4$), and killed 24 h after injection. All major organs were collected and used for RNA extract. qRT-PCR was taken to detect the expression level of miR-143, and U6 was set as control. $^{**}P < 0.01$

The therapeutic outcome was also analyzed in terms of animal survival. Results showed that CL-pVAX-miR-143 treatments significantly prolonged the survival time (median, 162 days for CL-pVAX-miR-143 (1 mg/kg) treatment and 134 days for CL-pVAX-miR-143 (0.5 mg/kg) treatment, compared with 5% Glc treatment (median, 88 days) ($P < 0.01$). In addition, an increased benefit was also reflected in CL-pVAX-miR-143 (1 mg/kg) treatment compared with cisplatin treatment (median, 117 days) ($P < 0.05$) (Fig. 3e).

During the survival trial, various degrees of cancer metastasis were observed in some mice in the late period (Fig. 3f, Table 1). About 90 days after the last treatment, extreme weight loss and obvious tumor metastasis in leg, head, back or somewhere else were observed in some mice of the control groups (5% Glc or CL-pVAX groups), while less and smaller tumor metastasis and better survival status were observed in CL-pVAX-miR-143-treated mice during the same period (Fig. 3e, Table 1). The results indicated that CL-pVAX-miR-143 could inhibit tumor metastasis and prolong the survival time in the early-stage experimental A549 lung cancer metastasis mice model, and the therapeutic effects showed to be dose dependent.

Systemic delivery of CL-pVAX-miR-143 inhibited tumor metastasis in lung cancer xenografts at advanced stage

To further evaluate the tumor suppression effect of CL-pVAX-miR-143 in the advanced lung cancer metastasis model, we built a model of advanced experimental A549 lung cancer metastasis mice. 7 weeks after lung cancer cells engraftment, part of the mice exhibited weight loss, and some even showed tumor metastasis in legs or tails (Fig. 4a). Especially, much more metastatic nodules were observed on the surface of the lung, which were signs of the advanced stage of lung cancer in mice (Li et al. 2011). Afterwards, those mice were randomly divided into different groups and received 5% Glc, CL-pVAX, different doses of CL-pVAX-miR-143 or cisplatin treatments, respectively.

Results showed that compared with 5% Glc treatment, the reductions of tumor metastasis nodules with treatment of cisplatin or CL-pVAX-miR-143 (0.5 mg/kg, 1 mg/kg) were 42.2%, 58.9% and 77.5%, respectively, which demonstrated

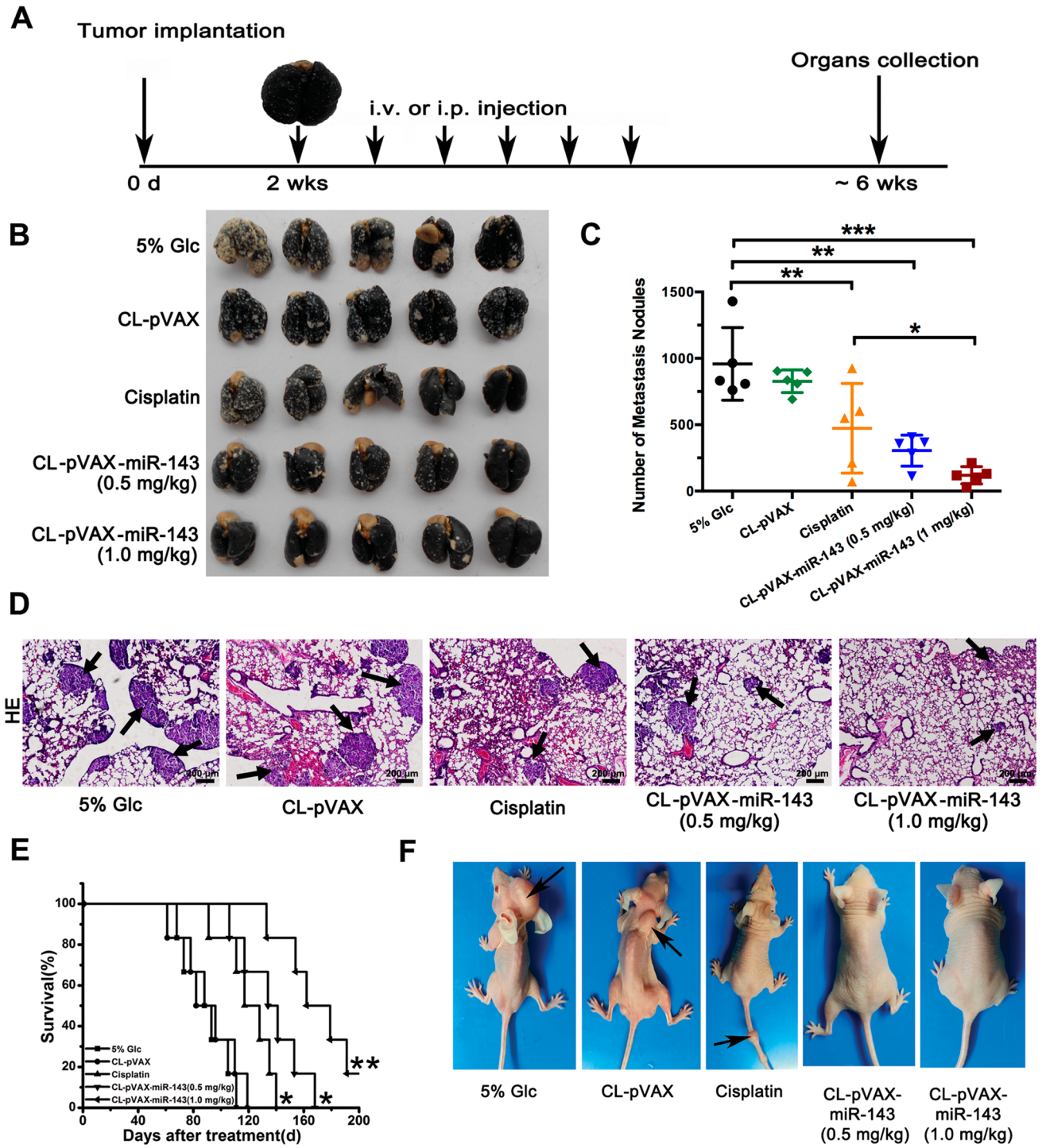

Fig. 3 Systemic delivery of CL-pVAX-miR-143 inhibited experimental lung metastasis tumor at early stage. **a** Timeline of CL-pVAX-miR-143 therapeutic delivery experiment; **b** photographs of lungs excised from the tumor-bearing mice; **c** The number of metastatic nodules in each group; **d** HE staining of lungs from each group. Scale bar: 200 μm; **e** survival analysis of A549 lung metastases-bearing mice; **f** representative images of mice from each group during survival. $^{*}P<0.05$, $^{**}P<0.01$, $^{***}P<0.001$

that treatment with cisplatin or different doses of CL-pVAX-miR-143 all showed obviously fewer and smaller metastatic nodules ($P<0.01$). In addition, the CL-pVAX-miR-143 (1 mg/kg) treatment showed an enhanced reduction compared with control treatment ($P<0.001$), and also showed statistical difference compared with cisplatin treatment

Table 1 Statistics of mice bearing surface metastatic tumor during survival ($n=6$)

Variables	5% Glc	CL-pVAX	Cisplatin	CL-pVAX-miR-143 (0.5 mg/kg)	CL-pVAX-miR-143 (1.0 mg/kg)
Early-stage group	5/6	4/6	3/6	2/6	1/6
Advanced- stage group	4/6	5/6	4/6	2/6	2/6

($P<0.05$) (Fig. 4b, c). Moreover, HE staining showed that the lung tissue treated with CL-pVAX-miR-143 contained much fewer and smaller metastatic nodules (Fig. 4d), and the therapeutic effect was also dose dependent.

In the survival trial, CL-pVAX-miR-143 treatment significantly prolonged the survival time of advanced experimental A549 lung cancer metastasis mice (Fig. 4e). The median survival times of 5% Glc and CL-pVAX groups were 48, 57 days, respectively, while the median survival times of cisplatin, CL-pVAX-miR-143 (0.5 mg/kg) and CL-pVAX-miR-143 (1 mg/kg) groups were 69, 87, 99 days, respectively. Compared with the controls, the other three groups all prolonged the survival time ($P<0.05$), and the CL-pVAX-miR-143 (1 mg/kg) group significantly prolonged the survival time ($P<0.01$). Moreover, an increased benefit was also shown in CL-pVAX-miR-143 (1 mg/kg) treatment compared to cisplatin treatment (Fig. 4e).

Besides, during the survival trial (~55 days after last treatment), when obvious weight loss or tumor metastasis induced by tumor development was observed in control group mice (5% Glc and CL-pVAX groups), the CL-pVAX-miR-143-treated mice still showed better survival status, and fewer tumor metastasis and less weight loss were observed. In addition, the CL-pVAX-miR-143 (1 mg/kg)-treated mice also showed better survival status and fewer tumor metastasis than the cisplatin-treated mice (Fig. 4f, Table 1). The results above indicated that CL-pVAX-miR-143 could significantly inhibit tumor metastasis and prolong the survival time of advanced A549 lung cancer metastasis models, and the therapeutic effect was also dose dependent.

Intratumoral delivery of CL-pVAX-miR-143 inhibited tumor growth in lung cancer xenografts

Tumor inhibition effect of CL-pVAX-miR-143 was also explored by intratumoral injection of CL-pVAX-miR-143 into A549 subcutaneous tumor. During the experimental period, rapid tumor growth was observed in 5% Glc and CL-pVAX groups, compared to the other groups. Moreover, CL-pVAX-miR-143-treated xenografts also displayed slower tumor growth compared to cisplatin-treated xenografts (Fig. 5a). At the end of the experiment, all the tumors were harvested to evaluate the therapeutic effects (Fig. 5b). Compared to 5% Glc treatment, CL-pVAX-miR-143 and cisplatin treatment could both significantly inhibit tumor growth by 53.4% and 44.6%, respectively ($P<0.01$). However, the inhibition effect of CL-pVAX-miR-143 group was greater than cisplatin treatment (Fig. 5c). The tumor weights were in agreement with the tumor growth inhibition (Fig. 5d).

Besides, histopathological analysis of the tumor tissues showed that dramatically visible responses with necrosis/apoptosis regions were observed in CL-pVAX-miR-143 and cisplatin-treated tumor tissues, compared with 5% Glc and CL-pVAX-treated tumor tissues, and more extensive areas of coagulative necrosis were observed in CL-pVAX-miR-143-treated tumor tissues than cisplatin-treated tumor tissues (Fig. 5e). Collectively, the results above suggested that CL-pVAX-miR-143 treatment could significantly inhibit the growth of A549 lung cancer xenografts, and showed a better therapeutic effect than cisplatin treatment.

Toxicology assessments

Multiple administrations are common ways to treat cancer in clinical practice (Schroeder et al. 2012). Thus, it is important to evaluate the accompanying side effect. To preliminarily assess the toxicity of CL-pVAX-miR-143, different groups were set including a group of double the effective dose (1 mg/kg). Before the administrations in each group, the weight of mice showed no significant difference. During the period of treatment, no unwanted side effects such as body weight changes, behavioral alterations and other signs of discomfort were observed in CL-pVAX-miR-143-treated (1 mg/kg and 2 mg/kg) mice as well as in 5% Glc and CL-pVAX groups, while an obvious weight loss was observed in the cisplatin treatment group (Fig. 6a). Besides, after a total of six administrations, the mice in the group of CL-pVAX-miR-143 treatment with a high dose (2 mg/kg) showed a better living status than those in cisplatin group (Fig. 6b). To evaluate the effects of CL-pVAX-miR-143 treatment on major organs after multiple administrations, the pathologic examination was taken by HE staining. The results showed that no pathological changes were observed in CL-pVAX-miR-143 treatment (1 mg/kg and 2 mg/kg) groups compared with the 5% Glc or CL-pVAX groups (Fig. 6c).

Moreover, to observe the effects of CL-pVAX-miR-143 treatment on liver and kidney after multiple administrations, levels of ALT, AST, and BUN in serum were also measured 24 h after the last injection. Results showed that compared with the 5% Glc or CL-pVAX groups, multiple

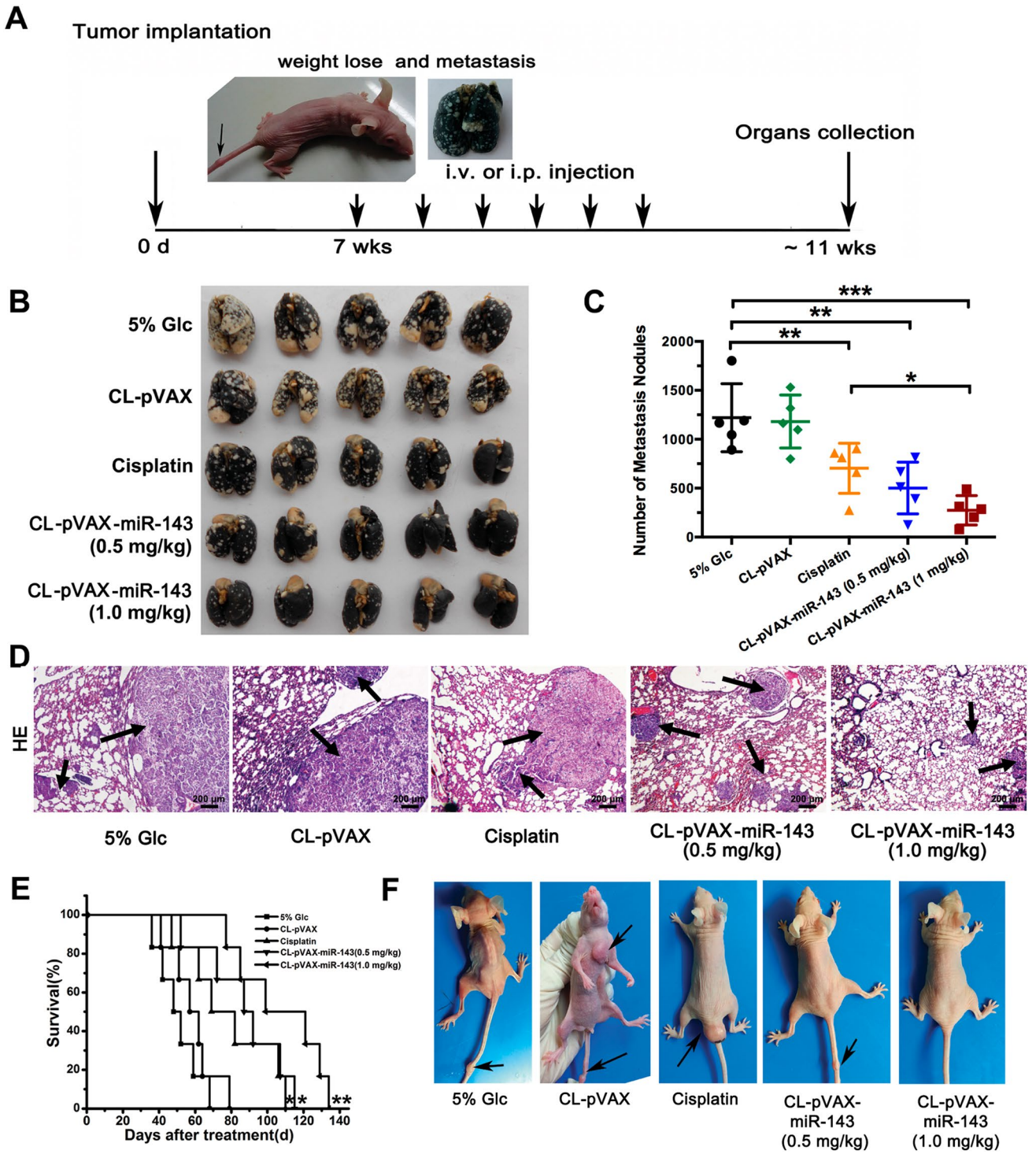

Fig. 4 Systemic delivery of CL-pVAX-miR-143 inhibited experimental lung metastasis tumor at advanced stage. **a** Timeline of CL-pVAX-miR-143 therapeutic delivery experiment; **b** photographs of lungs excised from the tumor-bearing mice; **c** the number of metastatic nodules in each group; **d** HE staining of lungs from each group. Scale bar: 200 μm; **e** survival analysis of A549 lung metastases-bearing mice. **f** Representative images of mice from each group during survival. $^{*}P<0.05$, $^{**}P<0.01$, $^{***}P<0.001$

administrations of CL-pVAX-miR-143 (1 mg/kg) did not induce significant production of ALT, AST, and BUN. Moreover, when the CL-pVAX-miR-143 treatment dose was increased twofold, the levels of ALT, AST and BUN were also not changed significantly, which indicated a lack of damage to the liver or kidney after multiple

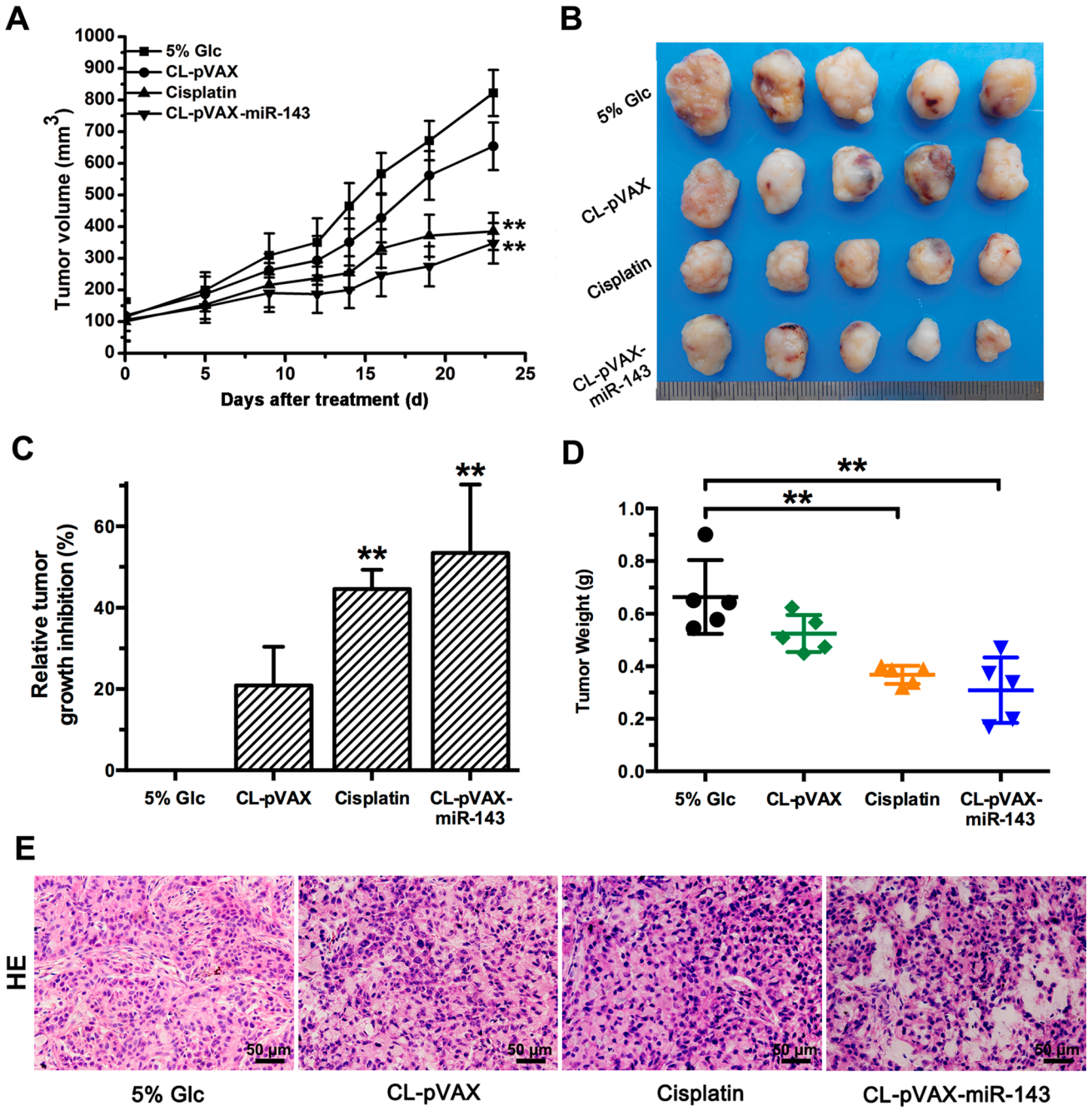

Fig. 5 Intratumoral delivery of CL-pVAX-miR-143 inhibited subcutaneous lung tumor growth. **a** Tumor volume in each group. The weight of the mice and the tumor volume were recorded every 3 days until animal was killed at day 23; **b** photograph of tumors at the end of the experiment; **c** relative tumor growth inhibition in each group; **d** the tumor weights in the indicated group; **e** HE staining of tumors in indicated groups. Scale bar: 50 μm. $^{*}P<0.05$, $^{**}P<0.01$

administrations of CL-pVAX-miR-143 (2 mg/kg). On the contrary, treatment with cisplatin showed obviously increase in the levels of ALT, AST, and BUN (Table 2). Taken together, these results demonstrated the safety and low toxicity for systemic delivery of CL-pVAX-miR-143 in vivo.

The preliminary mechanism on tumor inhibition of CL-pVAX-miR-143

To preliminarily explore the mechanism of CL-pVAX-miR-143 on tumor inhibition, the expression levels of miR-143 in subcutaneous tumor tissues were measured by

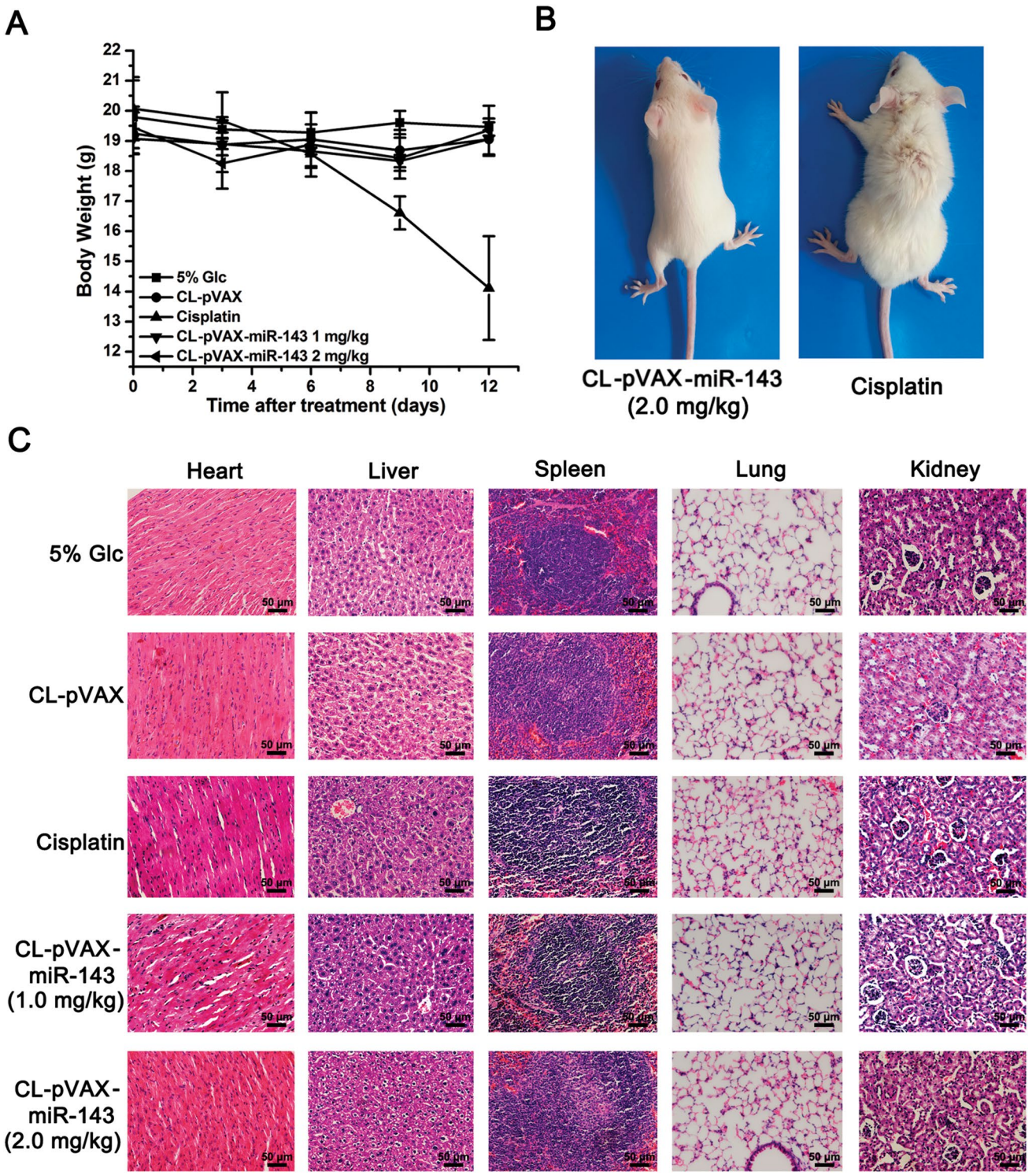

Fig. 6 Toxicity evaluation of CL-pVAX-miR-143 treatment in vivo. **a** Total body weight of mice during treatment in indicated groups; **b** representative images of the living status of mice from CL-pVAX-miR-143 (2 mg/kg) and cisplatin-treated group; **c** HE staining of mice in major organs in indicated groups. Scale bar: 50 μm

qRT-PCR firstly to confirm whether miRNA was successfully expressed in tumor tissues. The result showed that the expression levels of miR-143 were increased sixfold approximately, which indicated that miR-143 was expressed successfully after CL-pVAX-miR-143 treatment (Fig. 7a). In our previous study, we found that the mechanism of

Table 2 Biochemical parameters of continuous administration ($x \pm$ SD values)

Groups	AST (IU/L)	ALT (IU/L)	BUN (mg/dL)
5% Glc	134.5 ± 3.2	34.5 ± 4.9	15.23 ± 2.1
CL-pVAX	121.5 ± 6.7	44.3 ± 1.3	16 ± 3.4
Cisplatin	588.3 ± 12.1	240 ± 10	64.8 ± 5.8
CL-pVAX-miR-143 (1 mg/kg)	145.3 ± 4.4	35.7 ± 3.7	15.4 ± 1.4
CL-pVAX-miR-143 (2 mg/kg)	146 ± 6.7	45 ± 2.7	13.15 ± 2.1

Liver and kidney injuries were evaluated using AST, ALT, and BUN measurements ($n = 4$)

miR-143 inhibiting the migration and invasion of NSCLC might be through targeting CD44v3 (Ma et al. 2013). In the current study, systemic delivery of CL-pVAX-miR-143 also showed significantly inhibition on tumor metastasis in both early-stage and advanced experimental lung cancer metastasis models. Thus, western blotting was further performed to detect the expression of CD44v3 in tumor tissues. Results showed that CL-pVAX-miR-143 treatment leads to dramatically downregulation of protein levels of CD44v3 compared with the controls ($P < 0.01$) (Fig. 7b), which further indicated that the preliminary mechanism on CL-pVAX-miR-143 inhibiting tumor metastasis might be induced by targeting CD44v3. Since angiogenesis plays a critical role in the process of growth and metastasis of primary solid tumors, immunohistochemical staining of CD34 was carried out to evaluate the angiogenesis. The result unveiled that a significant reduction number of CD34-positive vessels was observed in CL-pVAX-miR-143-treated tumor tissue ($P < 0.001$) (Fig. 7c, f). In addition, the Ki-67 staining showed that CL-pVAX-miR-143 treatment strikingly reduced nuclear Ki-67 levels compared to 5% Glc and CL-pVAX treatment ($P < 0.001$, Fig. 7d, g). Meanwhile, an increased DNA fragmentation (green) in CL-pVAX-miR-143-treated tumor tissue was observed compared with the controls by Tunel staining, which indicated enhanced intratumoral apoptosis after CL-pVAX-miR-143 treatment ($P < 0.001$, Fig. 7e, h).Thus, we inferred that anti-tumor effects of CL-pVAX-miR-143 were also related with the suppression of cell proliferation, angiogenesis and the promotion of apoptosis.

Discussion

Lung cancer is of high incidence, often accompanied by cancer metastasis, and diagnosed at an advanced stage. Although there has been rapid development of novel biological therapies, lung cancer still remains the leading cause of cancer-related deaths worldwide, and improvements are urgently needed (Olaussen and Postel-Vinay 2016). In this study, we prepared CL-pVAX-miR-143 and found that CL-pVAX-miR-143 could effectively and safely inhibit tumor growth and tumor metastasis in vivo. Especially, CL-pVAX-miR-143 treatment significantly inhibited tumor metastasis and prolonged survival in early-stage and advanced A549 lung cancer metastasis models. Besides, CL-pVAX-miR-143 treatment showed greater anti-tumor effects than cisplatin in those NSCLC xenografts. Thus, our study suggested that CL-pVAX-miR-143 might be a novel and potential strategy for NSCLC therapy, especially for advanced NSCLC with metastasis.

In clinical practice, multiple systemic administration is an essential way to treat lung cancer (Schroeder et al. 2012). Naked miRNAs often face many obstacles like nuclease degradation, insufficient miRNA stability, and ineffective delivery before reaching the target site of activity (Hosseinahli et al. 2018). To solve these problems, a suitable vector is needed. Viral and non-viral vectors were frequently used in recent studies. However, viral vectors might be accompanied by the risk of recombination and strong immunogenicity (Ganju et al. 2017). Besides, viral vector often induced innate immunogenicity and failed to provide greater benefit by repeating administration (Shi et al. 2013). Compared with viral vectors, non-viral vectors were highly biocompatible, degradable, and easy to enlarge production (Fernandez-Pineiro et al. 2017; Ganju et al. 2017). Among non-viral vectors, cationic liposome was widely used in gene therapy (Fernandez-Pineiro et al. 2017), and the DOTAP/cholesterol (Chol)-based liposome could act as a delivery vector for therapeutic cancer vaccine (Verbeke et al. 2017) or cancer treatments (Muralidharan et al. 2016; Yan et al. 2018). In recent years, DOTAP/Chol liposome has been reported to deliver FUS1 in NSCLC in phase I/II clinical trials (Yin et al. 2014). Moreover, the efficiency of DOTAP/Chol-based cationic liposomes delivering genes to the lung and the therapeutic effects were observed in a series of studies (Hattori et al. 2015; Ito et al. 2004; Ramesh et al. 2001). Therefore, in our study, cationic lipid (DOTAP: cholesterol liposome) was used to condense miRNAs and form lipoplexes in an attempt to enhance the pharmacological effectiveness in vivo.

After conjunction of miR-143 with cationic liposome, we found that CL-pVAX-miR-143 could protect miR-143 plasmids from DNAse I and serum degradation in vitro while avoiding large blood cells aggregation and, thus, revealed low toxicity. Subsequently, in the biodistribution trial in vivo, miR-143 was identified to be mainly accumulated in the lung after systemic delivery of CL-pVAX-miR-143. Previous report revealed that this might be due to the affinity of the lipoplexes with lung capillary endothelial cells (Sakurai et al. 2001). In the toxicity studies, HE staining of the major organs (heart, liver, spleen, lung, and kidney) and biochemical parameters of ALT, AST, BUN

results showed that the mice did not show obvious toxicity after multiple administration of CL-pVAX-miR-143 at a twofold therapeutic dose. These findings indicated that the therapeutic dose of CL-pVAX-miR-143 in vivo would be safe for treatment. Thus, we inferred that it would be safe by systemic delivering the CL-pVAX-miR-143 with our therapeutic dose.

Some studies have reported the anticancer effects of miR-143 in some tumor models. miR-143 mimics could inhibit colorectal xenograft growth dose dependently (1.25 mg/kg and 2.5 mg/kg) by systemic administration (Akao et al. 2010). The growth of subcutaneous and orthotopic pancreatic cancer xenografts was significantly inhibited by systemic delivery of miR-143/145 plasmid (Pramanik et al. 2011). Likewise, systemic delivery of miR-143 agomir could inhibit tumor growth in xenograft mouse models of triple-negative breast cancer (Miao et al. 2016). Similar with those reports, in our study, intratumoral delivery of CL-pVAX-miR-143 significantly inhibited tumor growth, while systemic delivery of CL-pVAX-miR-143 significantly inhibited tumor metastasis and prolonged survival dose dependently in early-stage A549 lung cancer metastasis models.

It was reported that the vast majority of the NSCLC patients was diagnosed at an advanced stage accompanied by metastasis, and treatment with surgery or chemotherapy received limited benefits in those cases (Hirsch et al. 2016; Olaussen and Postel-Vinay 2016; Zugazagoitia et al. 2017). Given clinical considerations, research on advanced metastasis lung cancer is of great significance. Thus, we built advanced A549 lung cancer metastasis models and kept on exploring the therapeutic potential of CL-pVAX-miR-143 in advanced NSCLC. It has been reported that advanced lung cancer mice had evident tumor burden in the lungs, which was similar to cancer patients presenting with advanced inoperable lung cancer at diagnosis (Li et al. 2011). Besides, advanced lung cancer patients often showed weight loss, which suggested a poor signal of cancer development (Jafri et al. 2013; Simmons et al. 2015). In our study, we also observed those phenomena in those mice models. Moreover, a few mice were observed having some tumor metastasis in the leg, tail, or somewhere else. It showed that the A549 lung cancer metastasis models had come to an advanced stage. Besides, we observed that mice with cisplatin treatment in advanced stage lung cancer model showed relatively higher tumor metastasis rate. It suggested that the cisplatin could not receive a satisfactory result in lung cancer therapy at advanced stage. Differently, stronger tumor inhibition effect (0.5 mg/kg, 58.9% inhibition; 1 mg/kg, 77.5% inhibition) and superior survival (0.5 mg/kg, 87 days; 1 mg/kg, 99 days) were observed in advanced A549 lung cancer metastasis mice after CL-pVAX-miR-143 treatment, compared with cisplatin treatment (42.5% inhibition, median, 69 days). Hence, it indicated that CL-pVAX-miR-143 treatment might be a promising strategy in advanced NSCLC treatment.

Cisplatin is a front-line chemotherapy for NSCLC. However, the chemotherapy-related febrile neutropenia could lead to life-threatening events and was thus a common cause of treatment modification (Cupp et al. 2018). Besides, multiple clinical practices showed that most NSCLC patients would eventually develop resistance to the chemotherapeutic agents to which they were exposed, cisplatin included (Zang et al. 2017). Differently, miRNA was reported playing an important role in inhibiting drug resistance. It has been proved that miR-770 could suppress doxorubicin resistance in triple-negative breast cancer (Li et al. 2018). Besides, miR-148-3p reconstitution could sensitize cisplatin-resistance gastric cancer cells to cisplatin treatment (Li et al. 2017). Thus, miRNA therapy seemed to be more promising in cancer therapy. Compared to cisplatin, CL-pVAX-miR-143 took advantage not only in anti-tumor growth and metastasis effects but also in prolonging survival and keeping the mice a better physical condition, which indicated that CL-pVAX-miR-143 might be of great potential in cancer therapy.

Previously, we found that miR-143 could inhibit lung cancer cell migration and invasion significantly by targeting CD44v3 (Ma et al. 2013). Moreover, CD44v3 played important roles in tumor metastasis (Barbour et al. 2003; Zaiden et al. 2017). In the present study, systemic delivery of CL-pVAX-miR-143 significantly inhibited tumor metastasis in both early-stage and advanced experimental lung cancer metastasis models. Thus, we further detected the protein level of CD44v3 in tumors. Consistently, we preliminarily found that CD44v3 was low expressed in CL-pVAX-miR-143-treated tumor. However, whether CD44v3 plays the vital role in mediating the anti-tumor effect of CL-pVAX-miR-143 in NSCLC still needs to be further explored.

To this end, our study identified that CL-pVAX-miR-143 had effective and safe inhibition effects on NSCLC in vivo. Notably, systemic delivery of CL-pVAX-miR-143 significantly inhibited tumor metastasis and prolonged survival dose dependently in early-stage experimental lung cancer metastasis model. Especially, same results were shown in advanced experimental lung cancer metastasis model. Meanwhile, CL-pVAX-miR-143 showed greater benefit than cisplatin in those NSCLC xenografts. The preliminary mechanism of CL-pVAX-miR-143 on inhibiting tumor metastasis might be induced by targeting CD44v3. Besides, the anti-tumor effects of CL-pVAX-miR-143 were also related with the suppression of cell proliferation, angiogenesis and the promotion of apoptosis. Collectively, our study suggested that CL-pVAX-miR-143 might be a promising strategy for clinical treatment of NSCLC, especially for advanced NSCLC with metastasis.

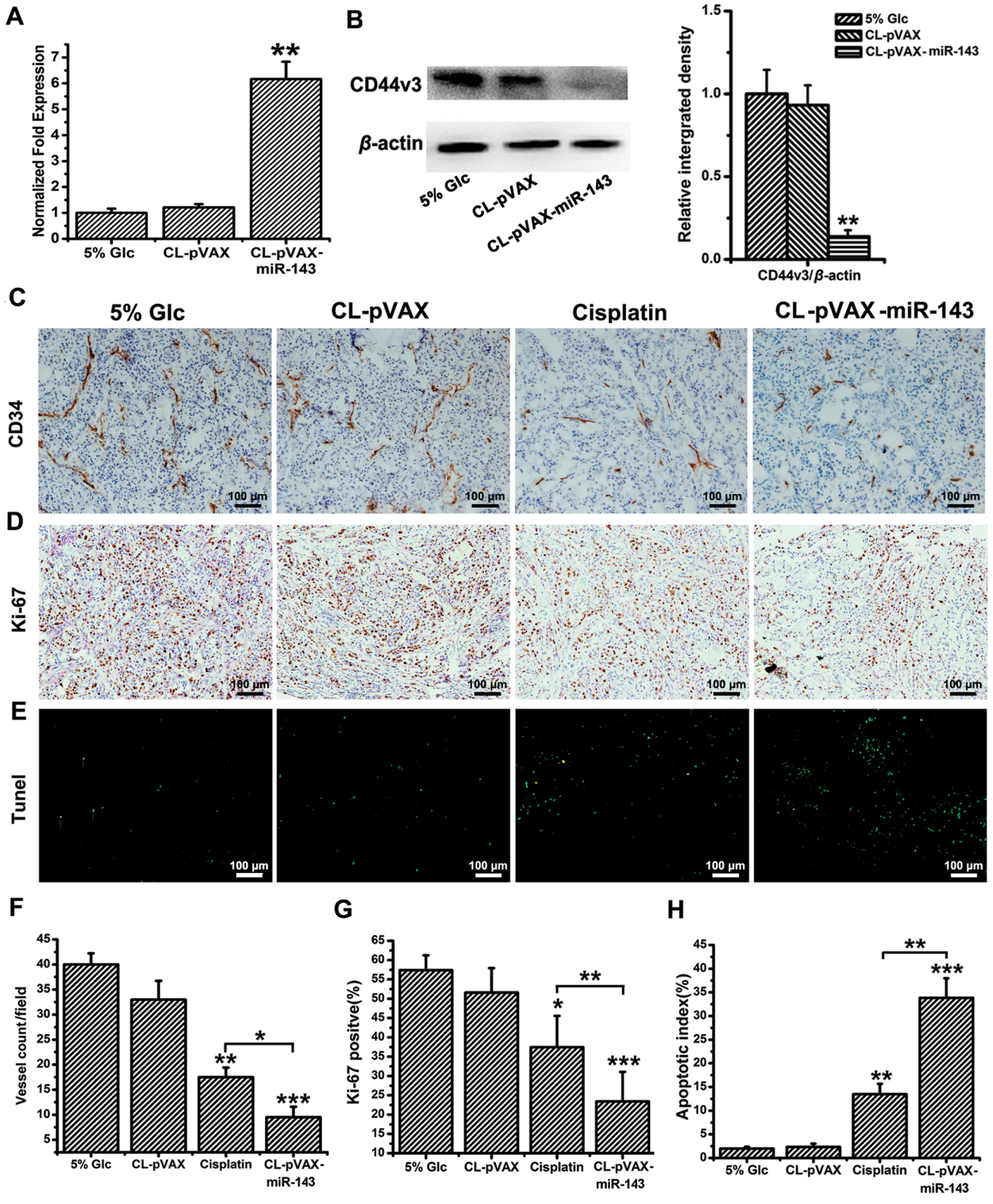
A
Normalized Fold Expression
**
5% Glc
CL-pVAX
CL-pVAX-miR-143
B
CD44v3
β-actin
5% Glc
CL-pVAX
CL-pVAX-miR-143
Relative intergrated density
5% Glc
CL-pVAX
CL-pVAX-miR-143
**
CD44v3/β-actin
C
5% Glc
CL-pVAX
Cisplatin
CL-pVAX-miR-143
CD34
100 μm
D
Ki-67
100 μm
E
Tunel
100 μm
F
Vessel count/field
*
**
***
5% Glc
CL-pVAX
Cisplatin
CL-pVAX-miR-143
G
Ki-67 positve(%)
*
**
***
5% Glc
CL-pVAX
Cisplatin
CL-pVAX-miR-143
H
Apoptotic index(%)
**
***
5% Glc
CL-pVAX
Cisplatin
CL-pVAX-miR-143

◂**Fig. 7** The mechanism of tumor growth and tumor metastasis inhibition by CL-pVAX-miR-143. **a** Relative expression of miR-143 detected by qRT-PCR in tumors collected from the mice with the indicated treatments; **b** (left) Western blot analysis of CD44v3 in indicated tumor tissues, β-actin was used as an internal control. (right) The relative integrated density of CD44v3 in indicated tumor tissues; **c** immunohistochemistry staining with CD34 in indicated tumor tissue sections. Scale bar: 100 μm; **d** Immunohistochemistry staining with Ki67 in indicated tumor tissue. Scale bar: 100 μm; **e** apoptosis in indicated tumor tissue sections detected with TUNEL assay. Scale bar: 100 μm; **f** the density of vessel in indicated tumor tissue sections. The number of vessels per × 100 field was counted; **g** the Ki-67 index in indicated groups; **h** the apoptotic index in indicated groups. $^{*}P < 0.05$, $^{**}P < 0.01$, $^{***}P < 0.001$

Materials and methods

Cell culture and experimental animals

The NSCLC cell line A549 was purchased from American Type Culture Collection (ATCC, Manassas, VA, USA), and cultured in 1640 medium (Gibco, Gaithersburg, USA) with 10% fetal bovine serum (FBS, Gibco, Gaithersburg, USA) in a humidified atmosphere containing 5% CO_2 at 37 °C. Female athymic nude mice of age 3–5 weeks and female Balb/c mice of 7–8 weeks were purchased from HFK Bioscience (Beijing, China) and were maintained in a specific pathogen-free (SPF) environment. All work performed on animals was in accordance with a protocol approved by the National Institutes of Health 'Guide for the Care and Use of Laboratory Animals' in Sichuan University.

Construction of miR-143-expressing plasmids

The miR-143 sequence was acquired from a pcDNA3.1-miR-143 plasmid and inserted into the BamH I/Xba I site in the pVAX plasmid vector (Invitrogen, Carlsbad, CA, USA) (termed as pVAX-miR-143). All the sequences were confirmed by DNA sequencing. Plasmid DNA was purified as described in the EndoFree plasmid purification handbook (Qiagen, Germantown, MD, USA).

Preparation of CL-pVAX-miR-143

Empty cationic liposomes (CL) were prepared firstly by dissolving DOTAP (Avanti Polar Lipids, Alabaster, AL, USA) and cholesterol (Merck, Darmstadt, Germany) at a 1:1 molar ratio in a mixture of ethanol. Subsequently, the organic solvent was removed, and the remaining dried film of lipid was then kept under high vacuum overnight to ensure complete removal of the organic solvent. 5% Glc was then added to the vacuum-dried lipid film and the mixture was allowed to hydrate for 30 min, then the mixture was ultrasonically disrupted for 10 min and filtered by 0.22 μm filter.

The cationic liposome/pVAX-miR-143 complexes (CL-pVAX-miR-143) were prepared by mixing the positively charged liposome and negatively charged miR-143 plasmid on a weight ratio basis according to the previous studies (Ou et al. 2012; Thapa et al. 2016). Then, the mixture was incubated at room temperature for 30 min and used immediately.

The agarose gel electrophoresis retardation assay was conducted to evaluate the DNA encapsulation efficiency of the cationic liposome. Different weight ratios of pVAX-miR-143 plasmid and cationic liposome were mixed and tested in the agarose gel electrophoresis. Particle sizes and zeta potentials of CL-pVAX-miR-143 were measured at 25 °C by the Zetasizer Nano ZS90 (Malvern Instrument, Malvern, UK). Besides, EGFP plasmids were taken to mix with cationic liposome in the transfection experiment for testing the transfection efficiency of the cationic liposome.

Characterization of CL-pVAX-miR-143

Details of serum degradation assays were as described earlier (Rodriguez et al. 2012). Briefly, a sample of pVAX-miR-143 plasmid or CL-pVAX-miR-143 was, respectively, mixed with fresh FBS (Gibco, Gaithersburg, USA) in a 1:1 ratio to give 50% serum concentration. The mixtures were then incubated at 37 °C for the indicated times (10 min, 20 min, 60 min, 120 min). Aliquots from each mixture sample were mixed with 5% Triton, separately, and then analyzed by electrophoresis.

DNase I protection assays were performed by incubating pVAX-miR-143 plasmid or CL-pVAX-miR-143 with DNase I (Fermentas, Ontario, Canada), 0.25 U/1 μg plasmid. The mixtures were then incubated at same indicated times with serum degradation assays and 0.5 M EDTA was then added to terminate the digestion. Aliquots from each mixture sample were separately mixed with 5% Triton and then analyzed by electrophoresis.

The blood cell aggregation experiments were performed by incubating CL-pVAX-miR-143 in 0.5% blood cell suspension at 37 °C for 10 min. Untreated blood cells and cells incubating with cationic liposome were set as controls to evaluate the anti-blood cell aggregation effect.

Biodistribution of systemically delivered CL-pVAX-miR-143

To evaluate the biodistribution of CL-pVAX-miR-143 after systemic administration, female Balb/c mice were given a single dose of 1 mg/kg CL-pVAX-miR-143 or an equal volume of 5% Glc intravenously. After 24 h, mice were killed and major organs were removed to frozen in liquid nitrogen immediately. RNA was isolated from all tissues. Then, the

expression levels of miR-143 in major organs (heart, liver, spleen, lung, and kidney) were detected using qRT-PCR (Daige et al. 2014).

Systemic delivery of CL-pVAX-miR-143 in metastatic lung cancer xenografts

To evaluate the therapeutic effect of CL-pVAX-miR-143 in early-stage lung cancer, early-stage metastatic lung cancer mice model was built by i.v. injection with A549 cells (3×10^6/200 µl) in female athymic nude mice of 3 weeks old. Two weeks after cell injection, mice were randomly divided into five groups ($n = 14$): 5% Glc, CL-pVAX, CL-pVAX-miR-143 (0.5 mg/kg), CL-pVAX-miR-143 (1 mg/kg), cisplatin (2 mg/kg), and received i.v. injection, respectively, with 5% Glc or different doses of CL-pVAX-miR-143 or i.p. injection of cisplatin every 2 days for a total of six injections. Two weeks after the last injection administration, eight mice were picked out randomly from each group and anesthetized.

Lungs of three mice in each group were excised and fixed in 4% buffered paraformaldehyde for further pathological analysis. Lungs of another five mice in each group were intratracheally injected with Indian ink and fixed in AAF solution (85% ethanol, 10% acetic acid, 5% formalin) to evaluate metastatic tumor nodules on lung surfaces. The relative metastatic inhibition ratio was calculated in terms of the tumor nodules in the designed treatment group relative to that of 5% Glc control group. The other six mice in each group were monitored daily for mortality since the last injection. Mice survival curves were plotted according to the Kaplan–Meier method.

To evaluate the therapeutic effect of CL-pVAX-miR-143 on advanced lung cancer, advanced metastatic lung cancer mice model was built by i.v. injection with A549 cells (3×10^6/200 µl) in female athymic nude mice of age 3 weeks old. 7 weeks after A549 cells engraftment, part of the mice exhibited weight loss, and tumor metastasis was observed in the leg or tail of some mice. Meanwhile, much more metastatic nodules were found on the surface of the lung by injecting the mice intratracheally with Indian ink. Then, those advanced metastatic lung cancer mice were randomly divided into five groups ($n = 14$): 5% Glc, CL-pVAX, CL-pVAX-miR-143 (0.5 mg/kg), CL-pVAX-miR-143 (1 mg/kg), cisplatin (2 mg/kg), and received same treatment as described above.

Intratumoral delivery of CL-pVAX-miR-143 in subcutaneous lung cancer xenografts

A549 cells (5×10^6/200 µl) were injected into the flanks of 5-week-old female *nu/nu* mice to generate subcutaneous xenografts. One week after the injection of tumor cells, subcutaneous tumor volumes (V) were measured with digital calipers (Fisher Scientific) and calculated using the formula: $V(\text{mm}^3) = 0.52 \times \text{length (mm)} \times \text{width}^2$ (mm^2). Treatment was initiated when the mean tumor volume had reached about 100 mm^3. Mice were randomly divided into four groups ($n = 8$): 5% Glc, CL-pVAX, and CL-pVAX-miR-143 (1 mg/kg), cisplatin (2 mg/kg) and received intratumoral injection, respectively, with 5% Glc or different liposome complexes or i.p. injection of cisplatin every 2 days for a total of six injections. 24 h after the last injection, three mice were picked out randomly from each group and anesthetized by ether inhalation. Then, tumor tissues were harvested and immediately fixed in 4% paraformaldehyde for paraffin embedding or snap frozen for RNA preparation or western blot analysis.

Tumor sizes of the other five mice were measured twice weekly. When the average tumor volume of the control group had reached about 1000 mm^3 or the tumors were necrotic, all the mice in each group were anesthetized, and tumor tissues were peeled off for photographs. The relative tumor growth ratio was calculated by the change of tumor volumes in designed treatment relative to that of 5% Glc control group.

Toxicity studies

To preliminarily assess the toxicity of CL-pVAX-miR-143, the Balb/c mice (7–8 weeks) were randomly divided into five groups ($n = 4$): 5% Glc, CL-pVAX, CL-pVAX-miR-143 (1 mg/kg), CL-pVAX-miR-143 (2 mg/kg), cisplatin (2 mg/kg), and received i.v. injection, respectively, with 5% Glc or different doses of CL-pVAX-miR-143 or i.p. injection of cisplatin every 2 days for a total of six injections. 24 h after the last injection, blood samples were collected and the serum was separated to measure the biochemical indicators (AST, ALT, BUN). Major organs (heart, liver, spleen, lung, and kidney) were excised and fixed in 4% buffered paraformaldehyde for further pathological analysis.

Quantitative PCR of miR-143

Quantitative real-time PCR (qRT-PCR) was taken to measure the expression of miR-143 in tissues. Total RNA for qRT-PCR analysis was extracted using Trizol (Invitrogen, Carlsbad, CA) according to the manufacturer's instructions, then reverse-transcribed into cDNA with the PrimeScript™ RT-PCR Kit (Takara Biotech, Dalian, China). QRT-PCR was conducted according to the procedures reported previously (Ma et al. 2013). Expression of miR-143 with relative to U6 was determined using the $2^{-\Delta\Delta Ct}$ method.

Western blot analysis

Total protein was extracted from A549 subcutaneous tumor tissues by the procedure following the manufacturer's protocol. Protein concentrations were determined with a modified Lowry protein assay kit (Thermo Scientific, Fremont, CA, USA). Western blot was then performed using standard immunoblotting protocols. The antibodies used were anti-human CD44v3 (R&D Systems, Abingdon, UK), and anti-human β-actin (Santa Cruz, CA, USA). All the antibodies were diluted with TBS-T containing 5% bovine serum albumin and 0.01% sodium azide. β-actin was set as loading control by re-incubating the same membrane.

Histology and immunohistochemistry

Tissues immersed in 4% paraformaldehyde were finally embedded in paraffin. Staining with hematoxylin–eosin was performed using 4 μm tissue sections which were mounted on poly-lysine slides and stained with H&E. For immunohistochemistry staining, 4 μm thick A549 subcutaneous tumor slices were stained with the primary antibodies including rabbit anti-human Ki-67 (Cell Signaling Technology Beverly, MA, USA) and rat anti-mouse CD34 (Abcam, Cambridge, UK). Bright field images of all stained tissues were viewed on microscopy (Olympus, Tokyo, Japan). The percentage of Ki-67-positive cells was counted in five random fields. And the numbers of $CD34^+$ microvessels were determined according to the procedures reported previously (Weidner et al. 1991).

In situ TUNEL assay

To detect apoptotic cells in subcutaneous tumor tissues, sections of tumor tissue were manipulated with TUNEL assay using an in situ Cell Death Detection Kit (Promega, Madison, WI), following the manufacturer's protocol. The apoptotic index was calculated as the percentage of positively stained cells to the total cells in five randomly selected fields.

Statistical analysis

All statistical analysis was performed using SPSS 19.0 software. Data were presented as the mean values ± SD of at least 3 repeated experiments. The statistical significance was determined using one-way ANOVA and unpaired Student's *t* test. The animal survival data were analyzed using Kaplan–Meier survival analysis. P values < 0.05 were considered significant.

Compliance with ethical standards

Conflict of interest The authors declare that they have no conflict of interest.

Ethical standards This article does not contain any studies with human participants performed by any of the authors. All experiments involving animals were admitted and performed according to the requirements of the Institutional Animal Care and Use Committee of West China Hospital, Sichuan University.

References

Akao Y, Nakagawa Y, Hirata I et al (2010) Role of anti-oncomirs miR-143 and -145 in human colorectal tumors. Cancer Gene Ther 17:398–408

Barbour AP, Reeder JA, Walsh MD, Fawcett J, Antalis TM, Gotley DC (2003) Expression of the CD44v2-10 isoform confers a metastatic phenotype: importance of the heparan sulfate attachment site CD44v3. Cancer Res 63:887–892

Cioce M, Strano S, Muti P, Blandino G (2016) Mir 145/143: tumor suppressor, oncogenic microenvironmental factor or both? Aging-US 8:1153–1155

Cupp J, Culakova E, Poniewierski MS, Dale DC, Lyman GH, Crawford J (2018) Analysis of factors associated with in-hospital mortality in lung cancer chemotherapy patients with neutropenia. Clin Lung Cancer 19:e163–e169

Daige CL, Wiggins JF, Priddy L, Nelligan-Davis T, Zhao J, Brown D (2014) Systemic delivery of a miR34a mimic as a potential therapeutic for liver cancer. Mol Cancer Ther 13:2352–2360

Dimitrova N, Gocheva V, Bhutkar A et al (2016) Stromal expression of miR-143/145 promotes neoangiogenesis in lung cancer development. Cancer Discov 6:188–201

Dong YZ, Hu T (2018) Effects of miR-143 overexpression on proliferation, apoptosis, EGFR and downstream signaling pathways in PC9/GR cell line. Eur Rev Med Pharmacol Sci 22:1709–1716

Fernandez-Pineiro I, Badiola I, Sanchez A (2017) Nanocarriers for microRNA delivery in cancer medicine. Biotechnol Adv 35:350–360

Ganju A, Khan S, Hafeez BB, Behrman SW, Yallapu MM, Chauhan SC, Jaggi M (2017) miRNA nanotherapeutics for cancer. Drug Discov Today 22:424–432

Hattori Y, Nakamura A, Arai S, Kawano K, Maitani Y, Yonemochi E (2015) siRNA delivery to lung-metastasized tumor by systemic injection with cationic liposomes. J Liposome Res 25:279–286

He Z, Yi J, Liu X et al (2016) MiR-143-3p functions as a tumor suppressor by regulating cell proliferation, invasion and epithelial-mesenchymal transition by targeting QKI-5 in esophageal squamous cell carcinoma. Mol Cancer 15:51

Hirsch FR, Suda K, Wiens J, Bunn PA Jr (2016) New and emerging targeted treatments in advanced non-small-cell lung cancer. Lancet 388:1012–1024

Hirsch FR, Scagliotti GV, Mulshine JL, Kwon R, Curran WJ Jr, Wu YL, Paz-Ares L (2017) Lung cancer: current therapies and new targeted treatments. Lancet 389:299–311

Hosseinahli N, Aghapour M, Duijf PHG, Baradaran B (2018) Treating cancer with microRNA replacement therapy: a literature review. J Cell Physiol 233:5574–5588

Hossian A, Sajib MS, Tullar PE, Mikelis CM, Mattheolabakis G (2018) Multipronged activity of combinatorial miR-143 and miR-506 inhibits Lung Cancer cell cycle progression and angiogenesis in vitro. Sci Rep 8:10495

Iscaife A, Reis ST, Morais DR et al (2018) Treating metastatic prostate cancer with microRNA-145. Apoptosis 23:388–395
Ito I, Ji L, Tanaka F et al (2004) Liposomal vector mediated delivery of the 3p FUS1 gene demonstrates potent antitumor activity against human lung cancer in vivo. Cancer Gene Ther 11:733–739
Jafri SH, Shi R, Mills G (2013) Advance lung cancer inflammation index (ALI) at diagnosis is a prognostic marker in patients with metastatic non-small cell lung cancer (NSCLC): a retrospective review. BMC Cancer 13:158
Jin YP, Hu YP, Wu XS et al (2018) miR-143-3p targeting of ITGA6 suppresses tumour growth and angiogenesis by downregulating PLGF expression via the PI3 K/AKT pathway in gallbladder carcinoma. Cell Death Dis 9:182
Karmakar S, Kaushik G, Nimmakayala R, Rachagani S, Ponnusamy MP, Batra SK (2017) MicroRNA regulation of K-Ras in pancreatic cancer and opportunities for therapeutic intervention. Semin Cancer Biol 54:63–71
Lei C, Du F, Sun L et al (2017) miR-143 and miR-145 inhibit gastric cancer cell migration and metastasis by suppressing MYO6. Cell Death Dis 8:e3101
Li B, Torossian A, Li W et al (2011) A novel bioluminescence orthotopic mouse model for advanced lung cancer. Radiat Res 176:486–493
Li B, Wang W, Li Z et al (2017) MicroRNA-148a-3p enhances cisplatin cytotoxicity in gastric cancer through mitochondrial fission induction and cyto-protective autophagy suppression. Cancer Lett 410:212–227
Li Y, Liang Y, Sang Y et al (2018) MiR-770 suppresses the chemoresistance and metastasis of triple negative breast cancer via direct targeting of STMN1. Cell Death Dis 9:14
Lu J, Zhan Y, Feng J, Luo J, Fan S (2018) MicroRNAs associated with therapy of non-small cell lung cancer. Int J Biol Sci 14:390–397
Ma Q, Jiang Q, Pu Q et al (2013) MicroRNA-143 inhibits migration and invasion of human non-small-cell lung cancer and its relative mechanism. Int J Biol Sci 9:680–692
Miao Y, Zhang LF, Guo R et al (2016) (18)F-FDG PET/CT for monitoring the response of breast cancer to miR-143-based therapeutics by targeting tumor glycolysis. Mol Ther Nucleic Acids 5:e357
Muralidharan R, Babu A, Amreddy N et al (2016) Folate receptor-targeted nanoparticle delivery of HuR-RNAi suppresses lung cancer cell proliferation and migration. J Nanobiotechnol 14:47
Noguchi S, Mori T, Hoshino Y et al (2011) MicroRNA-143 functions as a tumor suppressor in human bladder cancer T24 cells. Cancer Lett 307:211–220
Olaussen KA, Postel-Vinay S (2016) Predictors of chemotherapy efficacy in non-small-cell lung cancer: a challenging landscape. Ann Oncol 27:2004–2016
Ou W, Ye S, Yang W et al (2012) Enhanced antitumor effect of cisplatin in human NSCLC cells by tumor suppressor LKB1. Cancer Gene Ther 19:489–498
Pramanik D, Campbell NR, Karikari C, Chivukula R, Kent OA, Mendell JT, Maitra A (2011) Restitution of tumor suppressor microRNAs using a systemic nanovector inhibits pancreatic cancer growth in mice. Mol Cancer Ther 10:1470–1480
Ramesh R, Saeki T, Templeton NS et al (2001) Successful treatment of primary and disseminated human lung cancers by systemic delivery of tumor suppressor genes using an improved liposome vector. Mol Ther 3:337–350
Rodriguez BL, Li X, Kiguchi K, DiGiovanni J, Unger EC, Cui Z (2012) Control of solid tumor growth in mice using EGF receptor-targeted RNA replicase-based plasmid DNA. Nanomedicine (Lond) 7:475–491
Rupaimoole R, Slack FJ (2017) MicroRNA therapeutics: towards a new era for the management of cancer and other diseases. Nat Rev Drug Discov 16:203–222
Sakurai F, Nishioka T, Yamashita F, Takakura Y, Hashida M (2001) Effects of erythrocytes and serum proteins on lung accumulation of lipoplexes containing cholesterol or DOPE as a helper lipid in the single-pass rat lung perfusion system. Eur J Pharm Biopharm 52:165–172
Schroeder A, Heller DA, Winslow MM et al (2012) Treating metastatic cancer with nanotechnology. Nat Rev Cancer 12:39–50
Shi HS, Yang LP, Wei W et al (2013) Systemically administered liposome-encapsulated Ad-PEDF potentiates the anti-cancer effects in mouse lung metastasis melanoma. J Transl Med 11:86
Siegel RL, Miller KD, Jemal A (2019) Cancer statistics, 2019. CA Cancer J Clin 69:7–34
Simmons CP, Koinis F, Fallon MT et al (2015) Prognosis in advanced lung cancer—a prospective study examining key clinicopathological factors. Lung Cancer 88:304–309
Skjefstad K, Johannessen C, Grindstad T et al (2018) A gender specific improved survival related to stromal miR-143 and miR-145 expression in non-small cell lung cancer. Sci Rep 8:8549
Steeg PS (2006) Tumor metastasis: mechanistic insights and clinical challenges. Nat Med 12:895–904
Thapa B, Plianwong S, Remant Bahadur KC, Rutherford B, Uludag H (2016) Small hydrophobe substitution on polyethylenimine for plasmid DNA delivery: optimal substitution is critical for effective delivery. Acta Biomater 33:213–224
van Zandwijk N, Pavlakis N, Kao SC et al (2017) Safety and activity of microRNA-loaded minicells in patients with recurrent malignant pleural mesothelioma: a first-in-man, phase 1, open-label, dose-escalation study. Lancet Oncol 18:1386–1396
Verbeke R, Lentacker I, Wayteck L et al (2017) Co-delivery of nucleoside-modified mRNA and TLR agonists for cancer immunotherapy: restoring the immunogenicity of immunosilent mRNA. J Control Release 266:287–300
Võsa VU, Vooder T, Kolde R, Vilo J, Metspalu A, Annilo T (2013) Meta-analysis of microRNA expression in lung cancer. Int J Cancer 132:2884–2893
Wang Y, Costanza F, Li C, Nimmagadda A, Song D, Cai J (2016) PEG-poly(amino acid)s/microRNA complex nanoparticles effectively arrest the growth and metastasis of colorectal cancer. J Biomed Nanotechnol 12:1510–1519
Wang K, Chen M, Wu W (2017) Analysis of microRNA (miRNA) expression profiles reveals 11 key biomarkers associated with non-small cell lung cancer. World J Surg Oncol 15:175
Weidner N, Semple JP, Welch WR, Folkman J (1991) Tumor angiogenesis and metastasis–correlation in invasive breast carcinoma. N Engl J Med 324:1–8
Yan H, Guo W, Li K et al (2018) Combination of DESI2 and endostatin gene therapy significantly improves antitumor efficacy by accumulating DNA lesions, inducing apoptosis and inhibiting angiogenesis. Exp Cell Res 371:50–62
Yin H, Kanasty RL, Eltoukhy AA, Vegas AJ, Dorkin JR, Anderson DG (2014) Non-viral vectors for gene-based therapy. Nat Rev Genet 15:541–555
Zaiden M, Feinshtein V, David A (2017) Inhibition of CD44v3 and CD44v6 function blocks tumor invasion and metastatic colonization. J Control Release 257:10–20
Zang H, Peng J, Wang W, Fan S (2017) Roles of microRNAs in the resistance to platinum based chemotherapy in the non-small cell lung cancer. J Cancer 8:3856–3861
Zer A, Leighl N (2014) Promising targets and current clinical trials in metastatic non-squamous NSCLC. Front Oncol 4:329

Zhai W, Sun Y, Guo C et al (2017) LncRNA-SARCC suppresses renal cell carcinoma (RCC) progression via altering the androgen receptor(AR)/miRNA-143-3p signals. Cell Death Differ 24:1502–1517

Zheng F, Liao YJ, Cai MY et al (2015) Systemic delivery of microRNA-101 potently inhibits hepatocellular carcinoma in vivo by repressing multiple targets. PLoS Genet 11:e1004873

Zugazagoitia J, Molina-Pinelo S, Lopez-Rios F, Paz-Ares L (2017) Biological therapies in nonsmall cell lung cancer. Eur Respir J 49:1601520